Optics Communications 282 (2009) 4676–4682

Contents lists available at ScienceDirect

Optics Communications

journal homepage: www.elsevier.com/locate/optcom

Compact photonic delay line constructed by holographic optical elements

Jiun-Shiou Deng [a,*], Ming-Feng Lu [a], Yang-Tung Huang [b]

[a] Department of Electronic Engineering, Minghsin University of Science and Technology, No. 1, Hsinshing Rd., Hsinfeng, Hsinchu 304, Taiwan
[b] Department of Electronics Engineering and Institute of Electronics, National Chiao Tung University, Hsinchu 300, Taiwan

ARTICLE INFO

Article history:
Received 10 June 2009
Received in revised form 28 August 2009
Accepted 28 August 2009

Keywords:
Photonic delay line
Holographic optical element
Polarization beam splitter
Signal-to-noise ratio
Balanced loss

ABSTRACT

To fully support phased-array antenna and other applications, a 3-range (long time, moderate time, and short time) delay line structures with holographic optical elements is proposed. Flexibility, light-weight, on-axis coupling, easy alignment, easy fabrication, and compactness are their advantages. When use holographic optical elements to build the photonic delay line system, all of the delay and non-delay paths in these three photonic delay lines are setting in a compact structure. They do not need any extra components, such as mirrors and optical paths in free space, and can bear stronger vibration. Therefore, the holographic optical elements are more suitable to design the photonic delay lines. In these three structures, their losses and crosstalk s are balanced. All of delay and non-delay cases in these three delay line structures, their crosstalk, signal-to-noise ratio, and loss are 1/81,000, 59.1 dB, and 3.2 dB, respectively. Finally, to support complete applications, a polarization independent photonic delay line system with holographic optical elements is proposed, too.

1. Introduction

The subject of variable photonic delay lines (PDLs) for phased-array antennas and other applications has become a key photonic-research area. Application of PDLs in microwave antenna signal processing offers some important advantages when compared with electronic processing. These advantages include large instantaneous and tunable signal-processing bandwidth and protection from electromagnetic interference and electromagnetic pulses [1–4]. PDLs that use a wide variety of devices and technologies [5] have been proposed and demonstrated such as Fourier-optic beamforming [6–8], fiber-optic RF phase control [9,10], integrated-optic RF phase control [11–13], acousto-optic liquid-crystal phase based beamforming [14,15], RF phase control via optical injection locking of microwave oscillator [16–18], integrated optical switching based time delays [19–21], fiber based time delays [22–24], bulk optical polarization switched signal control [1–4,25–28], wavelength multiplexed time delay systems [29,30], programmable optical delay lines using bulk acousto-optics [31,32], and micro-electro mechanical systems (MEMS) [33], photonic crystal [34], and other new technologies.

Holographic optical elements (HOEs) have polarization-dependent characteristics. With suitable designs, highly polarization-selective HOEs can be designed and fabricated [35–43]. The flexibility, light-weight, on-axis coupling, easy alignment, easy fabrication, and compactness are their advantage features. Using compactness feature and employing the same technology as Ref. [28], a PDL system with holographic-based can be compacted to bear vibrations. Using the totally internal reflection (TIR) technology to reduce the size of PDL systems with prism-based components [4] and using holographic-based components to construct PDL systems [44,45] have been proposed. In this paper, HOEs with TIR characteristic will be proposed to build a PDL system, in which both of delay and non-delay paths can be fit in a compact size. The whole system does not need any extra components, such as mirrors and optical paths in free space. Therefore, they can bear stronger vibration.

2. Holographic optical elements

In this section, two types of 1×2 holographic PBSs as shown in Figs. 1 and 2, respectively, will be discussed in detail. In each 1×2 holographic PBS, two conjugate polarization-selective holographic gratings (HG) are formed on two sides of a dielectric substrate. The difference between these two kinds of holographic PBSs is only that the dimension of the output holographic grating (HG_O) in the second one is smaller than the first one's. When the input optical beam is normally incident on the input holographic grating (HG_I), the Bragg reconstruction input angle is 0° and the diffraction angle inside the film medium is θ_D. On the other hand, the reconstruction angle is θ_D and the output diffracted optical beam is also normal to the HG_O. Based on Kogelnik's coupled wave theory for a volume type of grating [46], the diffraction efficiencies of *s*- and *p*-polarization fields with respect to the grating plane, η_s and η_p, are given as

* Corresponding author. Tel.: +886 3 5593142x3160; fax: +886 3 5591402.
E-mail address: djs@must.edu.tw (J.-S. Deng).

0030-4018/$ - see front matter © 2009 Elsevier B.V. All rights reserved.
doi:10.1016/j.optcom.2009.08.061

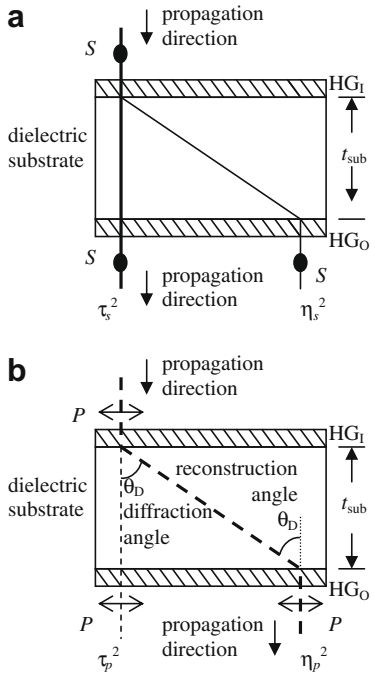

Fig. 1. The first type of 1×2 holographic PBS, where HG_I, HG_O, and t_{sub} are the input holographic grating, the output holographic grating, and the corresponding thickness of the dielectric substrate, respectively, and the wide solid line, wide dash line, narrow solid line, and narrow dash line are the *s*-polarized signal, *p*-polarized signal, *s*-polarized noise, *p*-polarized noise, respectively.

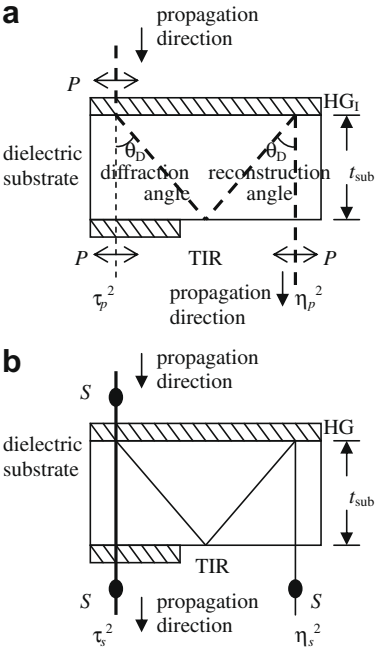

Fig. 2. The second type of 1×2 holographic PBS, where TIR is the total internal reflection.

$$\eta_s = \sin^2 v_s, \tag{1}$$

and

$$\eta_p = \sin^2 v_p, \tag{2}$$

where the modulation parameters, v_s (*s*-polarization) and v_p (*p*-polarization) are given as

$$v_s = \frac{\pi n_g d_g}{\lambda\sqrt{\cos\theta_D}}, \tag{3}$$

and

$$v_p = v_s \cos\theta_D = \frac{\pi n_g d_g \sqrt{\cos\theta_D}}{\lambda}, \tag{4}$$

respectively, where λ, d_g, and n_g are the operating wavelength, the thickness of the grating film, and the index modulation of the grating, respectively. Based on Eqs. (3) and (4), suitable value for θ_D and $n_g d_g/\lambda$ can be solved, as shown in Table 1, to obtain high polarization-selective property (0%- and 100%-diffraction for *s*- and *p*-polarization fields, respectively, or 0%- and 100%-diffraction for *p*- and *s*-polarization fields, respectively), and these devices have been designed and some were fabricated [35–43]. The values in Table 1 are the ideal cases. The experimental values of τ_s and η_p are great than 90% and η_s and τ_p are less than 3% [35].

Using the *s*-transmission/*p*-diffraction gratings ($\theta_D = 60.0°$ or 41.4°) in the structure shown in Fig. 1a as an example, when the input optical beam is *s*-polarized, the direction of this optical beam will not be changed by the input and output coupling holographic gratings (HG_I and HG_O). Therefore, the input channel connects to the output channel O_1 and the device performs the function of "*straight*" connection (direct transmission). In this case, most of the *s*-polarized optical power from the input channel passes directly through HG_I and HG_O to the output channel O_1. This part of optical power at the output channel O_1 is the desired signal and its transmission efficiency is $\tau_s^2 P_{in}$. Some *s*-polarized optical power from input channel will be diffracted by HG_I and HG_O to the output channel O_2. This part of optical power at the output channel O_2 is the undesired noise and its diffraction efficiency is $\eta_s^2 P_{in}$. Therefore, the crosstalk (ε) of the 1×2 holographic PBS in the "*straight*" state is

$$\varepsilon = \frac{\eta_s^2}{\tau_s^2} = \frac{1}{900}. \tag{5}$$

When the input optical beam is *p*-polarized, the input optical beam is diffracted by HG_I and normally coupled out with a conjugate diffraction by HG_O. Hence, the input channel connects to the output channel O_2 and the device performs the function of "*turn*" connection (diffraction) as shown in Fig. 1b. In this situation, some *p*-polarized optical power from the input channel passes directly through HG_I and HG_O to the output channel O_1. This part of optical power at the output channel O_1 is the undesired noise and its transmission efficiency is $\tau_p^2 P_{in}$. Most of the *p*-polarized optical power from the input channel will be diffracted and reconstructed by HG_I and HG_O, respectively, to output channel O_2. This part of optical power at the output channel O_2 is the desired signal and its diffraction efficiency is $\eta_p^2 P_{in}$. Therefore, the crosstalk (ε) of the 1×2 holographic PBS in the "*turn*" state can be derived as

$$\varepsilon = \frac{\tau_p^2}{\eta_p^2} = \frac{1}{900}. \tag{6}$$

When an *s*-polarized incident optical beam is from the output channel O_1, it will passes directly through HG_O and HG_I. Therefore,

Table 1
Parameters of a polarization-selective grating with high polarization-selective property.

v_s	π	$3\pi/2$	2π
v_p	$\pi/2$	π	$3\pi/2$
η_s (%)	0	100	0
η_p (%)	100	0	100
θ_D	60.0°	48.2°	41.4°
$\cos^{-1}(v_p/v_s)$	$\cos^{-1}(1/2)$	$\cos^{-1}(2/3)$	$\cos^{-1}(3/4)$
$n_g d_g/\lambda$	0.707	1.22	1.73

this *s*-polarized optical beam from the output channel O_1 will follow the same path backward and finally reach the input channel. Because HG_I and HG_O are conjugate, these two opposite direction optical paths between the input channel and the output channel O_2 are symmetry. Hence, the backward *p*-polarized optical beam will pass the same path from the output channel O_2 to the input channel. Obviously, this 1×2 holographic PBS provides a bi-directional switching function. Therefore, this 1×2 holographic PBS can also be operated as a 2×1 holographic beam combiner.

Fig. 2 shows the second type 1×2 holographic PBS. When the input optical beam is *p*-polarized, the input optical beam is diffracted by HG_I, reflected by the interface of the dielectric substrate, reconstructed by the same holographic grating (HG_I), and transmitted normally out the dielectric substrate. There is a total internal reflection (TIR) between the diffraction and reconstruction. These diffraction angles are greater than the critical angle in the dielectric substrate and the beam will be totally internal reflected. In this case, the device performs the function of "*turn*" connections (diffraction) as shown in Fig. 2a. The same as the situation of the type one, a part of optical power at the output channel O_1 is the undesired noise and its transmission efficiency is $\tau_p^2 P_{in}$, too. Most of the *p*-polarized optical power from the input channel will be diffracted and reconstructed by HG_I to output channel O_2. This part of optical power at the output channel O_2 is the desired signal and its diffraction efficiency is $\eta_p^2 P_{in}$. Hence, the crosstalk (ε) of the 1×2 holographic PBS in the "*turn*" state can be derived as

$$\varepsilon = \frac{\tau_p^2}{\eta_p^2} = \frac{1}{900}. \tag{7}$$

The same as the first type 1×2 holographic PBS, most of the *s*-polarized optical power from the input channel passes directly through HG_I and HG_O to the output channel O_1, when the input optical beam is *s*-polarized in the second type of the 1×2 holographic PBS as shown in Fig. 2b. This part of optical power at the output channel O_1 is the desired signal and its transmission efficiency is $\tau_s^2 P_{in}$. Some *s*-polarized optical power from input channel will be diffracted and reconstructed by HG_I to output channel O_2. This part of optical power is the undesired noise at the output channel O_2 and its diffraction efficiency is $\eta_s^2 P_{in}$. Hence, the crosstalk (ε) of the 1×2 holographic PBS in the "*straight*" state is

$$\varepsilon = \frac{\eta_s^2}{\tau_s^2} = \frac{1}{900}. \tag{8}$$

Similarly, the backward *s*-polarized or *p*-polarized optical beam will go through the same path propagating the forward beam from the original output channel to the original input channel. Obviously, the 1×2 holographic PBS is a bi-directional device, which can act as a 2×1 beam combiner also.

3. Polarization-dependent PDL with HOEs

To fully support for phased-array antenna and other applications, the delay line system needs several different delay time components [27]. To construct these wide range delay lines, it requires 3-range (long time, moderate time, and short time) delay line structure. In the delay and non-delay cases of PDLs, the insertion losses have to be balanced [26] and the signal-to-noise ratios (SNRs) have to be improved [3,44]. These requirements are very important characteristics of a PDL system. In this section, all structures have the same designs.

In this section, the long time (>5 ns), moderate time (5 ns ~ 0.1 ns), and short time (<0.1 ns) polarization-dependent PDLs composed of HOEs will be presented. To getting balanced loss and signal-to-noise ratio (SNR) in delay and non-delay cases, symmetry structures will be employed. Each kind of delay line consists of two electro-optic halfwave plates (EOHWPs) and two 1×2 holographic PBSs. All of the signals and noises in delay and non-delay cases of these three kinds of delay lines pass through the same numbers of EOHWPs and holographic gratings. Therefore, their losses and SNRs are balanced. In this section, the *s*-transmission/*p*-diffraction grating will be used. In this example, the initial input and final output beams remain *s*-polarized.

3.1. Short time delay

Fig. 3 shows a short time (<0.1 ns) polarization-dependent PDL, which consists of two EOHWPs and two first type 1×2 holographic PBSs. These two 1×2 holographic PBSs have opposite diffraction directions. For clear description, the non-delay and delay paths are denoted by points A and B, respectively. In the non-delay case, these two EOHWPs are inactive. Most of the *s*-polarized input optical signal passes directly through these EOHWPs and 1×2 holographic PBSs, and propagates along the path input → $EOHWP_1$ → HG_1 → HG_2 → A → HG_3 → HG_4 → $EOHWP_2$ → output. The length of the optical path is $2 \times t_{EOHWP} \times n_{EOHWP} + 2 \times t_{sub} \times n_{sub}$ and the transmission efficiency is $\eta_{EOHWP}^2 \times \tau_s^4$, where t_{EOHWP}, n_{EOHWP}, t_{sub}, n_{sub}, η_{EOHWP}, and τ_s are the thickness of the EOHWP, reflection index of the EOHWP, thickness of the dielectric substrate, reflection index of the dielectric substrate, transmission efficiency of the EOHWP, and transmission efficiency of the

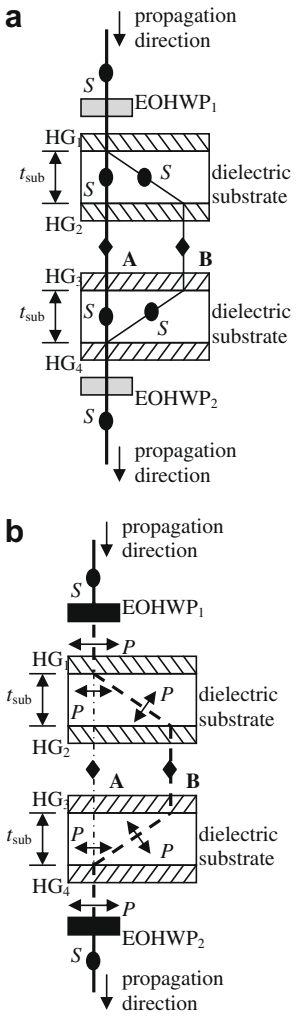

Fig. 3. Polarization-dependent short time photonic delay line with HOEs.

s-polarized field in the holographic grating, respectively. The optical power loss can be calculated as

$$\mathrm{IL} = 10\log_{10}\frac{1}{\eta_{\mathrm{EOHWP}}^2 \times \tau_s^4} = 3.2\ (\mathrm{dB}), \tag{9}$$

where η_{EOHWP} is 0.85 [26]. In this situation, a part of s-polarized optical signal will be turned by these two holographic PBSs to output along the other path: input → $\mathrm{EOHWP_1}$ → $\mathrm{HG_1}$ → $\mathrm{HG_2}$ → B → $\mathrm{HG_3}$ → $\mathrm{HG_4}$ → $\mathrm{EOHWP_2}$ → output, and its transmission efficiency is $\eta_{\mathrm{EOHWP}}^2 \times \eta_s^4$. Because this optical path is longer than another, this part of power arrives at the output at different time. Therefore, this part of s-polarized optical power is noise and SNR can be calculated as

$$\mathrm{SNR} = 10\log_{10}\left(\frac{\eta_{\mathrm{EOHWP}}^2 \times \tau_s^4}{\eta_{\mathrm{EOHWP}}^2 \times \eta_s^4}\right) = 10\log_{10}\left(\frac{\tau_s}{\eta_s}\right)^4 = 59.1\ (\mathrm{dB}). \tag{10}$$

In delay case, these two EOHWPs are active. After the s-polarized input optical signal passing through $\mathrm{EOHWP_1}$, the input optical signal will be changed to p-polarization. Most of the p-polarized optical signals will be turned to another direction by the upper 1×2 holographic PBS, pass point B, and turn back to output by the lower 1×2 holographic PBS. Its length of the optical path is $2 \times t_{\mathrm{EOHWP}} \times n_{\mathrm{EOHWP}} + 2 \times t_{\mathrm{sub}} \times \csc\theta_{\mathrm{D}} \times n_{\mathrm{sub}}$ and the transmission efficiency is $\eta_{\mathrm{EOHWP}}^2 \times \eta_p^4$, where the θ_{D} and η_p are the diffraction angle and the diffraction efficiency of the p-polarized field in the holographic grating, respectively. Therefore, the delay time can be calculated as

$$\Delta t_{\mathrm{S}} = \frac{2 \times (\csc\theta_{\mathrm{D}} - 1) \times t_{\mathrm{sub}} \times n_{\mathrm{sub}}}{C}, \tag{11}$$

where C is the optical velocity, and the optical power loss can be calculated as

$$\mathrm{IL} = 10\log_{10}\frac{1}{\eta_{\mathrm{EOHWP}}^2 \times \eta_p^4} = 3.2\ (\mathrm{dB}). \tag{12}$$

When the delay time (Δt_{S}) is 10 ps and the diffraction angle (θ_{D}) is 60°, the thickness of the dielectric substrates (t_{sub}) of these two 1×2 holographic PBSs only need 1 mm.

A part of p-polarized optical signal passes directly through EOHWPs and holographic PBSs to output along another path: input → $\mathrm{EOHWP_1}$ → $\mathrm{HG_1}$ → $\mathrm{HG_2}$ → A → $\mathrm{HG_3}$ → $\mathrm{HG_4}$ → $\mathrm{EOHWP_2}$ → output and the transmission efficiency is $\eta_{\mathrm{EOHWP}}^2 \times \tau_p^4$, where τ_p is the transmission efficiency of the p-polarized field in the holographic grating. The same reason, this optical path is shorter than the other's. This part of power arrives at the output at different time, too. Therefore, this part of p-polarized optical power is noise and SNR can be calculated as

$$\mathrm{SNR} = 10\log_{10}\left(\frac{\eta_{\mathrm{EOHWP}}^2 \times \eta_p^4}{\eta_{\mathrm{EOHWP}}^2 \times \tau_p^4}\right) = 10\log_{10}\left(\frac{\eta_p}{\tau_p}\right)^4 = 59.1\ (\mathrm{dB}). \tag{13}$$

3.2. Moderate time delay

Fig. 4 shows a moderate time (0.1 ns ~ 5 ns) polarization-dependent PDL, which consists of two second type 1×2 holographic PBSs as shown in Fig. 2 and two EOHWPs. In the non-delay case, these two EOHWPs are inactive. Most of the input optical signal passes directly through these EOHWPs and 1×2 holographic PBSs, and propagates along the path input → $\mathrm{EOHWP_1}$ → $\mathrm{HG_1}$ → $\mathrm{HG_2}$ → $\mathrm{HG_3}$ → $\mathrm{HG_4}$ → $\mathrm{EOHWP_2}$ → output. In this non-delay path, the length of the optical path is $2 \times t_{\mathrm{EOHWP}} \times n_{\mathrm{EOHWP}} + 2 \times t_{\mathrm{sub}} \times n_{\mathrm{sub}}$ and the transmission efficiency is $\eta_{\mathrm{EOHWP}}^2 \times \tau_s^4$, too. Hence, the optical power loss is the same as that of the short time delay PDL as shown in Eq. (9).

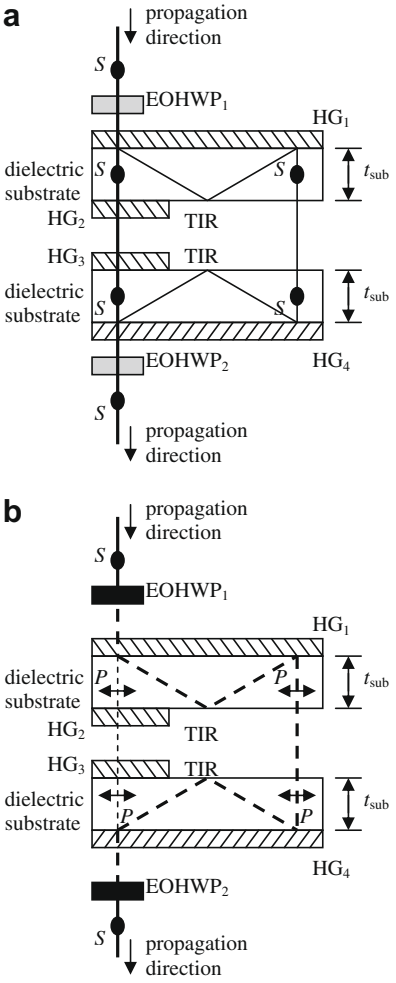

Fig. 4. Polarization-dependent moderate time photonic delay line, where TIR is total internal reflection.

In this case, a part of s-polarized optical signal will be turned by these two holographic PBSs to output along another path: input → $\mathrm{EOHWP_1}$ → $\mathrm{HG_1}$ → TIR → $\mathrm{HG_1}$ → $\mathrm{HG_4}$ → TIR → $\mathrm{HG_4}$ → $\mathrm{EOHWP_2}$ → output, and the transmission efficiency is $\eta_{\mathrm{EOHWP}}^2 \times \eta_s^4$. This part is undesired noise. Therefore, the SNR is the same as that of the short time delay PDL, too.

In the delay case, these EOHWPs are active. The s-polarized input optical signal is changed to p-polarized after passing through the $\mathrm{EOHWP_1}$. And then, most of the p-polarized optical power is diffracted by $\mathrm{HG_1}$. This diffracted optical signal follows the path to output: $\mathrm{HG_1}$ → TIR → $\mathrm{HG_1}$ → $\mathrm{HG_4}$ → TIR → $\mathrm{HG_4}$ → $\mathrm{EOHWP_2}$ → output. A total internal reflection is happen in both of the dielectric substrates of these two 1×2 holographic PBS. In this delay path, the length of the optical path is $2 \times t_{\mathrm{EOHWP}} \times n_{\mathrm{EOHWP}} + 4 \times t_{\mathrm{sub}} \times \csc\theta_{\mathrm{D}} \times n_{\mathrm{sub}} + 2 \times t_{\mathrm{sub}} \times n_{\mathrm{sub}}$ and the transmission efficiency is $\eta_{\mathrm{EOHWP}}^2 \times \eta_p^4$, too. Therefore, the optical power loss is the same as the short time delay PDL and the delay time is

$$\Delta t_{\mathrm{M}} = \frac{4 \times \csc\theta_{\mathrm{D}} \times t_{\mathrm{sub}} \times n_{\mathrm{sub}}}{C}. \tag{14}$$

As the diffraction angle (θ_{D}) is 41.4° and the delay time (Δt_{M}) is 1 ns, the thickness of the dielectric substrates (d_{sub}) need 3.75 cm.

A part of p-polarized optical signal passes directly through EOHWPs and holographic PBSs to output along another path: input → $\mathrm{EOHWP_1}$ → $\mathrm{HG_1}$ → $\mathrm{HG_2}$ → $\mathrm{HG_3}$ → $\mathrm{HG_4}$ → $\mathrm{EOHWP_2}$ → output and the transmission efficiency is $\eta_{\mathrm{EOHWP}}^2 \times \tau_p^4$, too. This part of the

p-polarized optical power is noise, too. Therefore, SNR can be calculated as short time delay PDL.

3.3. Long time delay

The structure of a long time (>5 ns) polarization-dependent PDL with HOEs is similar to the moderate time PDLs, except that the longer holographic grating of the first type 1×2 holographic PBS in the long time PDL has been divided into two segments as shown in Fig. 5. Therefore, these two structures have the same characteristics except the delay time. In the long time PDL, there are several TIRs to extend the optical path for getting longer delay. The delay time can be calculated as

$$\Delta t_L = \frac{2 \times (M+1) \times \csc\theta_D \times t_{sub} \times n_{sub}}{C}, \tag{15}$$

where M is the number of TIRs in a 1×2 holographic PBS. When the diffraction angle (θ_D), thickness of the dielectric substrate (t_{sub}), and delay time (Δt_L) are 41.4°, 3.75 cm, and 5 ns, respectively, the number of TIRs (M) is 9. In other words, the width of the dielectric substrates of the 1×2 holographic PBS in the long time PDL is 33.1 cm.

In fact, the delay time independs on the thickness of the dielectric substrate in this long time PDL. Compared with Fig. 5, the dielectric substrate thicknesses of the 1×2 holographic PBS of Fig. 6 has been reduced by half. In this situation, the number of TIRs has been increased from three to seven. In other words, as the number of TIRs is M while the dielectric substrate thickness is t_{sub}, the number of TIRs will increased to $2M + 1$ while the dielectric substrate thickness is reduced by half. At this time, the delay time can be calculated as

$$\Delta t'_L = \frac{2 \times (2M+1+1) \times \csc\theta_D \times \frac{t_{sub}}{2} \times n_{sub}}{C} = \frac{2 \times (M+1) \times \csc\theta_D \times t_{sub} \times n_{sub}}{C}. \tag{16}$$

As shown in Eqs. (15) and (16), the delay time is the same for two different thicknesses of the dielectric substrates. Combined two mirrors and three dielectric cubes, the dimension of the long time delay PDL can be reduced and still compact as shown in Fig. 7. In this figure, the diffraction directions of HG_5 and HG_6 have been changed. When the *p*-polarized optical signal reaches HG_5, the optical beam will be diffracted and coupled normally out the upper 1×2 holographic PBS. After passing these dielectric cubes and mirrors, the optical signal coupled normally into the lower 1×2 holographic PBS, diffracted by HG_6, and kept on the same

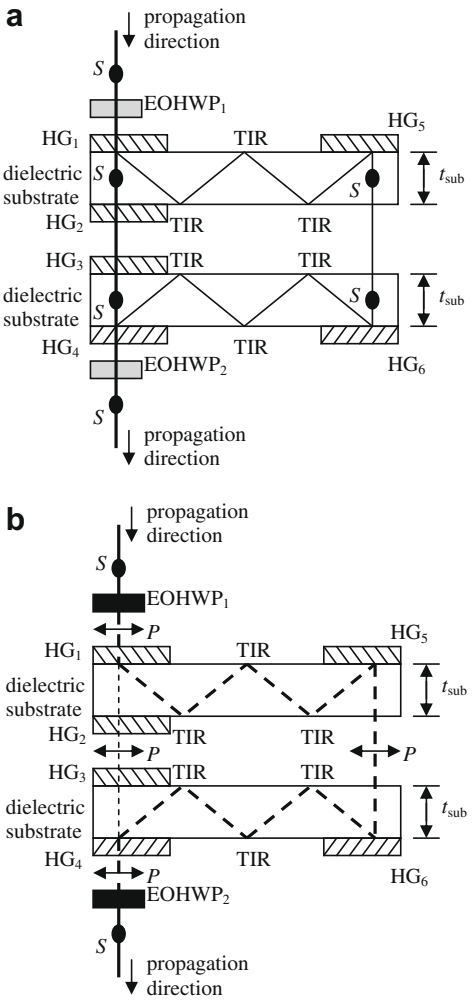

Fig. 5. Polarization-dependent long time photonic delay line.

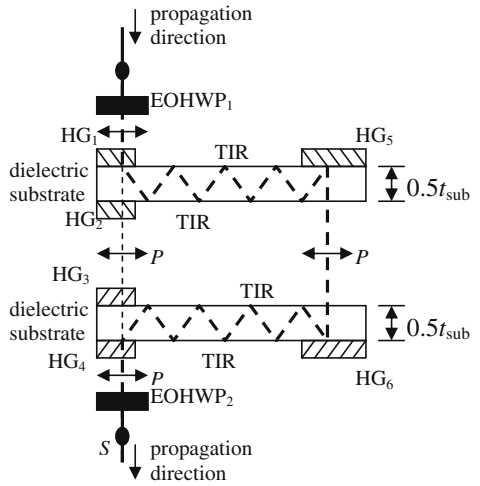

Fig. 6. The delay optical path of the polarization-dependent long time photonic delay line. In this structure, the thicknesses of the dielectric substrates have been reduced by half. The number of TIRs in a single substrate is seven.

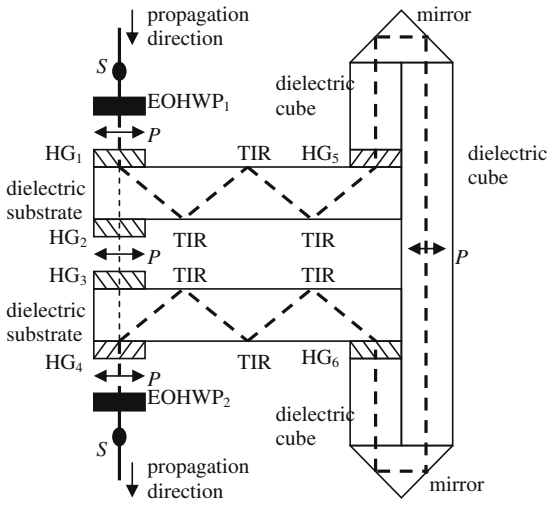

Fig. 7. Polarization-dependent long time photonic delay line with extra component to reduce the dimension.

optical path to output channel as shown in Fig. 5b. To get smaller dimension, pyramid design as shown in Ref. [4] is a more useful method.

All of the delay and non-delay paths, the optical signals from output channel will follow the same paths backward with corresponding polarizations and finally reach input channel. Therefore, three kinds of the photonic delay lines provide bi-directional transmission functions. Both delay and non-delay paths are setting in a compact structure. They do not need any extra components, such as mirrors, and optical paths in free space. Therefore, they can bear stronger vibration. However, its optical power loss is larger than prism-based PDL [4].

4. Polarization-independent PDLs with HOEs

In a polarization-dependent PDL system, the polarization of the input optical signal has to be fixed. Therefore, this system has to be cascaded a polarizer at the input for selecting a fixed polarization. However, the input optical signal power will be attenuated by the polarizer. In the worst case, differential phase is 90° and no input optical signal can pass through the polarizer. For example, the input and output optical signals have been fixed on *s*-polarization. When the input optical signal is *p*-polarized, whole input signal power will be completely blocked and its transmission efficiency is zero. For fully supporting all PDL applications, the polarization-independent PDL system has to be designed to resolve the major drawback of a polarization-dependent PDL system.

Fig. 8 shows the basic structure of the polarization-independent PDL with HOEs. This structure is based on the polarization-dependent PDL, which consists of a polarization-dependent PDL, two halfwave plates (HWPs), and two first type 1×2 holographic PBSs which the upper and lower one provide splitting and combining functions, respectively. In the other words, when the polarization-dependent PDL is a long time delay structure, this polarization-independent PDL is a long time delay structure, too. Both of these PDLs have the same delay time. The only difference between these two structures is the polarization characteristics: one is polarization-dependent and the other is polarization-independent.

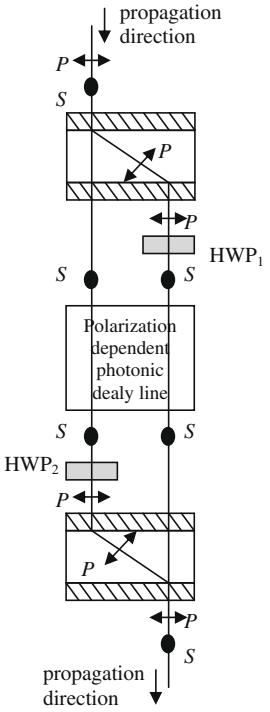

Fig. 8. The basic structure of a polarization-independent photonics delay line, where HWP is the halfwave plate.

From input channel to output channel, the *s*-polarization component passes directly through the upper 1×2 holographic PBS and the polarization-dependent PDL. After passing through HWP_2, its polarization will be changed into *p*-polarized and the transmission direction will be turned by the lower 1×2 holographic PBS to output.

The transmission direction of the *p*-polarization component is turned by the upper 1×2 holographic PBS and reach HWP_1. This *p*-polarization component will be changed into *s*-polarization, passed directly through the polarization-dependent PDL and the lower 1×2 holographic PBS to output, and combined with the other polarized component.

The transmission direction of these two polarized optical beams are symmetric and their optical path are $t_{HWP} \times (n_{HWP} + 1) + (\csc \theta_D + 1) \times t_{sub} \times n_{sub}$, where t_{HWP} and n_{HWP} are the thickness and reflection index of the halfwave plate, respectively. Because these two optical beams pass through the polarization-dependent PDL in parallel, they have the same optical path and arrive at output channel at the same time. Therefore, the differential optical path between these two polarized optical beams is zero. Due to that these two polarized optical beams are symmetric, these two polarized optical beams pass the same number of the 1×2 holographic PBSs and HWPs. Therefore, the losses of these two polarized optical beams are balanced.

Both of these two polarized optical beams from output channel will follow the same paths backward with corresponding polarizations and finally reach input channel. All of the polarization-independent PDLs provide bi-directional transmission functions, too.

5. Conclusion

To fully support phased-array antenna and other applications, a 3-range (long time, moderate time, and short time) delay line structures with balanced loss and signal-to-noise ratio constructed by holographic optical elements is proposed. Flexibility, lightweight, on-axis coupling, easy alignment, easy fabrication, and compactness are their advantages. When use holographic optical elements to build the photonic delay line system, all of the delay and non-delay paths in these three photonic delay lines are setting in a compact structure. All of delay and non-delay cases in these three delay line structures, their crosstalk, signal-to-noise ratio, and loss are 1/81,000, 59.1 dB, and 3.2 dB, respectively. They do not need any extra components, such as mirrors and optical paths in free space, and can bear stronger vibration. Therefore, the holographic optical elements are more suitable to design the photonic delay lines. Finally, to support complete applications, a polarization independent photonic delay line system with holographic optical elements is proposed, too.

Acknowledgement

This research was supported by Minghing University of Science and Technology under contract MUST-98I-1-3.

References

[1] N.A. Riza, IEEE J. Lightwave Technol. 12 (1994) 1440.
[2] N.A. Riza, IEEE Photon. Technol. Lett. 7 (1995) 1285.
[3] N.A. Riza, N. Madamopoulas, IEEE J. Lightwave Technol. 15 (1997) 1088.
[4] N. Madamopoulas, N.A. Riza, Appl. Opt. 37 (1998) 1407.
[5] N.A. Riza, Selected Papers on Photonic Control of Phased Array Antennas, SPIE Press, MS136, 1997.
[6] M. Tamburrini, M. Parent, L.G. Stillwell, Electron. Lett. 23 (1987) 680.
[7] E.N. Toughlian, H. Zmuda, P. Kornreich, IEEE Photon. Technol. Lett. 2 (1990) 444.
[8] Y. Konishi, W. Chujo, M. Fujise, IEEE Trans. Antennas Propag. 40 (1992) 1459.

[9] R. Benjamin, C.D. Zaglanikis, A.J. Seeds, Electron. Lett. 26 (1990) 1853.
[10] R. Benjamin, A.J. Seeds, IEE Proc. 1396 (1992) 526.
[11] R.A. Soref, J. Lightwave Technol. LT-3 (1985) 992.
[12] K. Horikawa, Y. Nakasuga, H. Ogawa, IEEE Trans. Theory Technol. 43 (1995) 2395.
[13] M.N. Armenise, V.M.N. Passaro, G. Noviello, Appl. Opt. 33 (1994) 6194.
[14] N.A. Riza, IEEE Photon. Technol. Lett. 4 (1992) 1072.
[15] N.A. Riza, J. Lightwave Technol. 10 (1992) 1974.
[16] B. Georges, K.Y. Lau, IEEE Photon. Technol. Lett. 5 (1993) 1344.
[17] S.T. Chew, T.K. Tong, M.C. Wu, T. Itoh, IEEE Microwave Guided Wave Lett. 4 (1994) 347.
[18] B. Ortega, J.L. Cruz, J. Capmany, M.V. Andres, D. Pastor, IEEE J. Lightwave Technol. 18 (2000) 430.
[19] S. Yegnanarayanan, P.D. Trinh, B. Jalali, Opt. Lett. 21 (1996) 740.
[20] Y. Chen, X. Zhang, R.-T. Chen, Proc. SPIE 4652 (2002) 249.
[21] Y. Chen, Ray T. Chen, Opt. Eng. 42 (2003) 2000.
[22] E.N. Toughlian, Henry Zmuda, Opt. Eng. 32 (1993) 613.
[23] D.A. Cohen, Y. Chang, A.F.J. Harold, R. Fetterman, Irwin L. Newberg, IEEE Photon. Technol. Lett. 8 (1996) 1683.
[24] Henry Zmu Richard A. Soref, Paul Payson, Steven Johns, Edward N. Toughlian, IEEE Photon. Technol. Lett. 9 (1997) 241.
[25] X.S. Yao, L. Maleki, IEEE Photon. Technol. Lett. 6 (1994) 1463.
[26] N. Madamopoulos, N.A. Riza, Opt. Commun. 152 (1988) 135.
[27] N. Madamopoulos, N.A. Riza, Appl. Opt. – IP 39 (2000) 4168.
[28] N.A. Riza, Proc. SPIE 2844 (1996) 274.
[29] A.P. Goutzoulis, D.K. Davies, Appl. Opt. 29 (1990) 5353.
[30] N.A. Riza, N. Madamopoulos, Appl. Opt. 36 (1997) 983.
[31] W.D. Jemison, P.R. Herczfeld, IEEE Microwave Guided Wave Lett. 3 (1993) 72.
[32] W.D. Jemison, T. Yost, P.R. Herczfeld, IEEE Microwave Guided Wave Lett. 6 (1996) 238.
[33] Shifu Yuan, Proc. SPIE 5201 (2003) 23.
[34] M. Fakharzadeh, O.M. Ramahi, S.-N. Safiedin, S.K. Chaudhuri, IEEE Trans. Adv. Pack. 31 (2008) 311.
[35] Y.-T. Huang, Y.-H. Chen, Opt. Lett. 18 (1993) 921.
[36] Y.-T. Huang, Y.-H. Chen, Optik 98 (1994) 41.
[37] J.-T. Chang, D.-C. Su, Y.-T. Huang, Appl. Opt. 33 (1994) 8143.
[38] Y.-T. Huang, Appl. Opt. 33 (1994) 2115.
[39] Y.-T. Huang, Opt. Lett. 20 (1995) 1198.
[40] J.-T. Chang, D.-C. Su, Y.-T. Huang, Appl. Phys. Lett. 68 (1996) 3537.
[41] Y.-T. Huang, M.-F. Lin, J.-S. Deng, K.-T. Fan, M.-J. Chang, Proc. SPIE 2885 (1996) 112.
[42] Y.-T. Huang, J.-S. Deng, D.-C. Su, J.-T. Chang, Opt. Mem. Neural Netw. 6 (1997) 249.
[43] J.-S. Deng, M.-F. Lu, C.-P. Lee, Y.-T. Huang, WSEAS Trans. Electron. 2 (2005) 33.
[44] N. Madamopoulos, N.A. Riza, Opt. Commun. 157 (1998) 225.
[45] Nicholas Madamopoulos, Nabeel A. Riza, Proc. SPIE 3388 (1998) 120.
[46] H. Kogelnik, Bell Syst. Tech. J. 48 (1969) 2909.